

1 **The neural substrates of how model-based learning**
2 **affects risk taking: functional coupling between right**
3 **cerebellum and left caudate**

4
5 Hangfeng Huo^{1,3,4,5}, Elise Lesage⁶, Wenshan Dong^{3,4,5}, Tom Verguts⁶, Carol A.
6 Seger^{3,4,5,9}, Sitong Diao², Tingyong Feng^{7,8*}, and Qi Chen^{2*}

7
8 ¹ Department of Psychology, Faculty of Education, Guangxi Normal University,
9 Guilin, China

10 ² School of Psychology, Shenzhen University, 518060 Shenzhen, China

11 ³ School of Psychology, South China Normal University, 510631 Guangzhou, China

12 ⁴ Center for Studies of Psychological Application, South China Normal University,
13 510631 Guangzhou, China

14 ⁵ Guangdong Key Laboratory of Mental Health and Cognitive Science, South China
15 Normal University, 510631 Guangzhou, China

16 ⁶ Department of Experimental Psychology, Ghent University, Ghent, Belgium

17 ⁷ Research Center of Psychology and Social Development, Faculty of Psychology,
18 Southwest University, Chongqing, China

19 ⁸ Key Laboratory of Cognition and Personality, Ministry of Education, Chongqing,
20 China

1 ⁹ Department of Psychology and Program in Molecular, Cellular, and Integrative
2 Neurosciences, Colorado State University, Fort Collins, Colorado, 80523, USA.

3

4

5 Please address correspondence to Qi Chen or Tingyong Feng:

6 Qi Chen,

7 School of Psychology

8 Shenzhen University

9 518060 Shenzhen

10 P.R. China

11 Email: chenqi@szu.edu.cn

12 Or

13 Tingyong Feng,

14 School of Psychology, Southwest University,

15 No.2, Tian Sheng RD., Beibei, Chongqing 400715, China

16 TEL: +86 23 68367572

17 Fax: +86 23 68253629

18 E-mail: fengty0@swu.edu.cn;

19

20

1

ABSTRACT

2

Higher executive control capacity allows people to appropriately evaluate risk and

3

avoid both excessive risk aversion and excessive risk-taking. The neural mechanisms

4

underlying this relationship between executive function and risk taking are still

5

unknown. We used voxel-based morphometry (VBM) analysis combined with

6

resting-state functional connectivity (rs-FC) to evaluate how one component of

7

executive function, model-based learning, relates to risk taking. We measured

8

individuals' use of the model-based learning system with the two-step task, and risk

9

taking with the Balloon Analogue Risk Task. Behavioral results indicated that risk

10

taking was positively correlated with the model-based weighting parameter ω . The

11

VBM results showed a positive association between model-based learning and gray

12

matter volume in the right cerebellum (RCere) and left inferior parietal lobule (LIPL).

13

Functional connectivity results suggested that the coupling between RCere and the

14

left caudate (LCAU) was correlated with both model-based learning and risk taking.

15

Mediation analysis indicated that RCere-LCAU functional connectivity completely

16

mediated the effect of model-based learning on risk taking. These results indicate that

17

learners who favor model-based strategies also engage in more appropriate risky

18

behaviors through interactions between reward-based learning, error-based learning

19

and executive control subserved by a caudate, cerebellar and parietal network.

20

Keywords: Decision making, Risk taking, Model-based learning, Functional

21

connectivity, Resting-state fMRI

1 **1 Introduction**

2 Life is full of decisions, and many come with risks. For instance, one may have
3 to decide whether to speed when there is a possibility of missing a plane, or whether
4 to adopt a financial manager's advice to purchase a stock. We are regularly faced with
5 many options that differ in potential for risk and/or loss. Risk taking behavior can
6 result in both positive gains and adverse outcomes. An individual's propensity for risk
7 taking impacts many real-life behaviors, such as financial investment choices, career
8 choices and professional success, unprotected sexual behaviors, substance abuse, and
9 extreme sports (Kuhnen & Knutson, 2005; Bleichrodt et al., 2018; Brymer &
10 Schweitzer, 2013; Derefinko et al., 2014; Tian et al., 2022). It is important to learn to
11 take an appropriate amount of risk: both excessive caution and excessive risk have
12 negative impact on our daily lives (Fecteau et al., 2007).

13 Risk taking is affected by many personality traits, including trait anxiety,
14 regulatory mode, and achievement motivation (Peters et al., 2020; Huo et al., 2020;
15 Panno et al., 2014; Pierro et al., 2008; Weinstein, 1969). Risk taking is also affected
16 by self-control and executive functions, such that people with higher executive
17 function capacity are able to overcome risk aversion to maximize potential gain (Blair
18 et al., 2018). One important cognitive function that requires executive function is
19 model-based learning. In model-based learning one deduces the underlying structure
20 of a situation and uses this mental model to make decisions, rather than deciding
21 solely on the basis of past reinforcement history (the latter is referred to as model-free

1 learning; Daw et al., 2011). In the current study we investigated potential neural
2 mechanisms underlying how individual differences in use of the model-based learning
3 strategy may be related to individual differences in risk taking.

4 **1.1 Risky decision making and model-based learning**

5 Previous research suggests that risky decisions rely on two functions, valuation
6 (evaluating different options) and selection (making the final choice according to the
7 result of valuation stage) (Ernst & Paulus, 2005; Kable & Glimcher, 2009). People
8 tend to prefer choices with certain outcomes over those that are risky and have a
9 potential for loss (Kahneman & Tversky, 1979), leading to risk aversion. Although
10 people are on average risk averse, some individuals exhibit excessive risk taking,
11 which has been associated with many adverse consequences including substance use
12 disorders (Verdejo-García et al., 2008). Achieving an appropriate level of risk taking
13 (one that maximizes positive outcomes and minimizes losses) requires a variety of
14 executive functions including reasoning ability (to learn what risks have payouts) and
15 cognitive control (to avoid impulsive risky decisions). Higher executive function
16 capacity promotes adaptive or successful participation in risk-taking actions (Romer
17 et al., 2017; Ogilvie et al., 2020).

18 One commonly used measure of risk taking is the Balloon Analogue Risk task
19 (BART), in which participants progressively inflate a balloon: higher inflation leads
20 to more reward, but also the risk of having the balloon burst resulting in no reward.
21 Previous research on this task has found that people with greater executive function

1 capacity, including higher working memory capacity, are able to learn and
2 consistently apply a strategy that maximizes reward (Blair et al., 2018). Ogilvie et al
3 (2020) found that BART performance was significantly associated with planning
4 executive functions and spatial working memory among young adults (aged 17 to 22
5 years). When the task is performed repeatedly, participants are able to learn across
6 trials what the best strategy is (van Ravenzwaaij et al., 2011; Lejuez et al., 2002).

7 One important aspect of executive functions that allows people to learn to make
8 appropriate decisions under conditions of risk is seen in model-based learning. An
9 influential paradigm developed by Daw et al (2011) distinguishes between model-free
10 and model-based processing. The model-based system builds and bases choices on a
11 causal model of the world, whereas the model-free system takes no account of the
12 causal structure. The model-based system learns to make more accurate decisions but
13 is computationally more expensive and slower than the model-free system. Model-
14 based learning can progress through testing different hypotheses about the structure of
15 the environment, a process which has significant executive control demands (Daw et
16 al., 2005; Janacsek et al., 2012; Otto et al., 2015). One aspect of executive function
17 that is critical for model-based learning is working memory (D'Esposito & Postle,
18 2015; Potter et al., 2017). Previous research has found that introducing a working
19 memory load during decision making reduces individuals' use of a model-based
20 strategy, and high working memory capacity protects model-based learning from
21 stress-induced impairment (Otto et al., 2013a; Otto et al., 2013b; Potter et al., 2017).

1 Other research has shown that improvement in model-based learning across
2 development can be predicted by development of fluid reasoning (Potter et al, 2017);
3 the construct of fluid reasoning has been shown to largely overlap that of executive
4 function (Decker et al., 2007). These well-established links between executive
5 function and risk-taking, and between executive function and model-based reasoning,
6 support our hypothesis that risk-taking and model-based reasoning themselves are
7 related. Interactions between model-based learning, executive function and risk-taking
8 may underlie the process of information selection in forming appropriate decision
9 strategy (Bechara et al., 2005; Kóbor et al., 2015).

10 Above we discussed how the type of reasoning processes utilized in model-based
11 learning task (e.g., hypothesis testing) require working memory and executive
12 function. However, the reader should note that reasoning is not limited to these types
13 of tasks, and not all forms of reasoning may have the same working memory and
14 executive function demands. Overall, reasoning is a process that inference from given
15 premises to form new conclusions (Castañeda et al., 2023). These inferences may
16 vary and can include deductive reasoning to draw new conclusions or assessment of
17 proposed conclusions (Johnson-Laird & Byrne, 1991; Ifenthaler, & Seel, 2013).

18 Mental models play a key part in all reasoning processes (Dayan et al., 2008;
19 Economides et al. 2015), but the need to manipulate and update these mental models,
20 and hence the need for working memory and executive function, may differ in
21 different situations.

1 **1.2 Neural systems underlying model-based learning and risky choice**

2 Consistent with the shared reliance on executive functions reviewed above, both
3 risky decision making and model-based learning rely on a common network
4 underlying executive function demanding tasks, recruiting lateral frontoparietal,
5 cerebellar, and caudate regions. Cortical regions in this network are collectively often
6 termed the multiple demand network (Duncan, 2010), within which the lateral
7 frontoparietal areas (dorsolateral prefrontal cortex and posterior parietal cortex) have
8 been shown to be particularly important for reasoning and rule-based learning
9 (Crittenden et al., 2016). The lateral frontoparietal system also interacts with
10 subcortical regions of the basal ganglia (Choi et al., 2012) and cerebellum (Buckner,
11 2013). Within the corticostriatal system, multiple demand regions interact primarily
12 with the dorsal caudate nucleus (Braunlich & Seger, 2013). The basal ganglia are
13 critical for reward-based instrumental learning (Doya, 1999, 2000; Lee et al., 2012;
14 Watabe-Uchida et al., 2017; Bostan & Strick, 2018), with the caudate nucleus
15 particularly important for using reward in the support of goal-directed learning (Seger,
16 2018). In addition, the lateral frontoparietal cortex interacts with the cerebellum in the
17 corticocerebellar network (Buckner 2013). The posterior cerebellum is connected to
18 prefrontal and parietal portions of the executive control network (Caulfield et al,
19 2016; O'Reilly et al, 2010) and is consistently activated by language and working
20 memory tasks (Lesage et al, 2010; Lesage et al, 2017).

1 The cerebellum is a key region for the formation of internal models used for both
2 movement and cognitive functions (Ito, 2008) such as predicting a long-term reward
3 during a Markov decision problem (Doya et al., 2001). The cerebellum compares
4 internal models with actual outcomes in a process of error-based learning (Doya,
5 1999, 2000; Bostan & Strick, 2018). Thus, the interconnections between
6 frontoparietal cortex, the basal ganglia and the cerebellum can collectively be
7 considered an executive control network underlying reasoning (Habas et al., 2009;
8 Braunlich & Seger, 2013; Bostan & Strick, 2018).

9 Both the BART and model-based reasoning tasks have been associated with this
10 frontoparietal-cerebellar-caudate executive control network. Gentili et al (2022)
11 identified individual differences in resting state measures of the amplitude of low
12 frequency fluctuations (ALFF) in the caudate nucleus and inferior parietal lobule was
13 associated with risk taking on subsequent performance of the BART. Reliance on
14 lateral frontoparietal cortex was associated with the choice to pump the balloon and
15 persisted across learning of the BART (Schonberg et al., 2012). Most fMRI studies of
16 model-based learning using the two-step task contrast it with model-free learning
17 rather than a neutral baseline tasks. Studies consistently find greater dorsal caudate
18 activity when behavior is driven by model-based reasoning (Huang et al., 2020) but
19 do not reliably report other multiple demand regions. The arbitration view of model-
20 based and model-free learning postulates that both functions occur in parallel with the
21 final response determined by a separate arbitration system; this parallel recruitment of

1 both functions could lead to similar neural recruitment (Lee et al., 2014). Other
2 methods find that lateral frontoparietal systems are important for model-based
3 learning. A voxel-based morphometry study found a region of prefrontal cortex where
4 grey matter density was associated with the model-based weighting parameter, ω
5 (Deserno et al., 2015). A TMS study found that interruption of PFC impaired model-
6 based reasoning (Smittenaar et al., 2013).

7 **1.3 The present study**

8 We investigated the relationship between model-based learning and risk taking
9 and their underlying neural substrates. Model-based learning and risk-taking were
10 measured using separate behavioral tasks (i.e., the two-step task and the Balloon
11 Analogue Risk Task (BART), respectively). We first assessed individuals' model-
12 based/model-free learning system using a two-step task (Kool et al., 2016) and
13 computational modeling, which allowed us to calculate for each participant their
14 model-based weighting parameter ω . We evaluated risk-taking using the BART
15 (Lejuez et al., 2002; Rao et al., 2008). In the BART, planning and working memory
16 functions are needed to learn and execute an appropriate strategy to maximize reward,
17 avoiding both excessive caution and excessive risk-taking (Ogilvie et al., 2020).

18 After the behavioral tasks, both voxel-based morphometry (VBM) and resting
19 state functional connectivity (rsFC) measures were used to study the underlying
20 neural substrates of model-based learning and risk taking. Specifically, we collected

1 anatomical image for VBM analyses and rsFC MRI images. We utilized VBM
2 analysis to identify brain areas in which gray matter (GM) volume associated with the
3 model-based learning weighting parameter ω . We predicted that these areas would be
4 within the executive control networks connecting the cerebellum, caudate, and lateral
5 frontoparietal cortex (in particular the dorsolateral prefrontal cortex and inferior
6 parietal lobule). We used these brain regions as seeds in a follow up voxel-wise rsFC
7 analysis to identify functionally connected neural networks, and then performed
8 correlation analyses to identify in which of these connection strengths correlated with
9 the behavioral measures of model-based reasoning and risk-taking. Finally, mediation
10 analyses tested whether functional connectivity in these networks mediated the
11 relationship between model-based reasoning and risk taking.

12 **2 Material and Methods**

13 **2.1 Participants and Procedure**

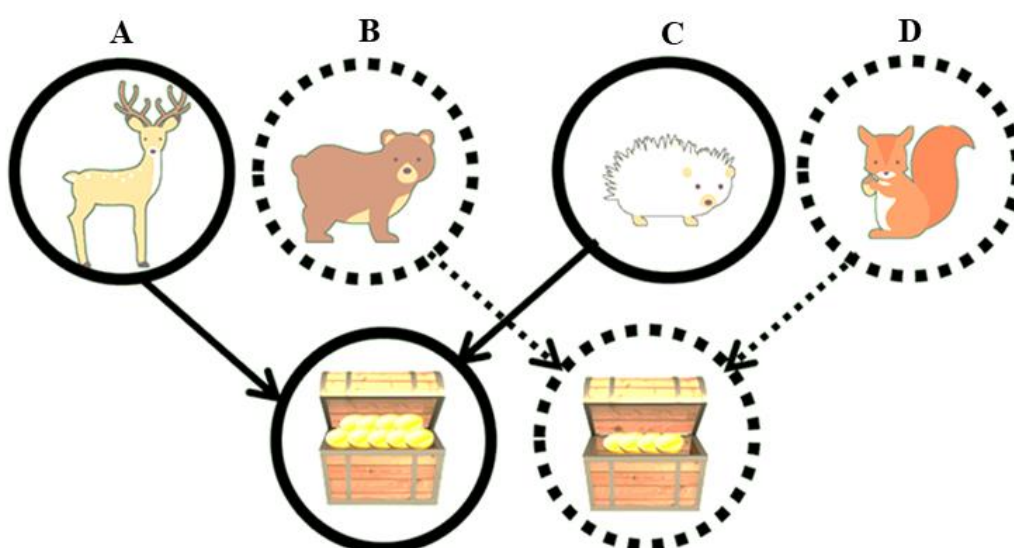
14 One hundred and ninety-one (55 males, 136 females; age 20.21 ± 1.60) college
15 students took part in the current study. All participants were recruited from Southwest
16 University. None of the participants reported brain damage, psychiatric or
17 neurological disease and all participants gave informed consent before MRI scanning.
18 All participants were told to stay calm and avoid excessive head motion (we used a
19 maximum head motion criterion of < 1.5 mm in translation and $< 1.5^\circ$ in rotation; all
20 participants met this standard and none were excluded). We also performed additional

1 motion scrubbing as detailed in the preprocessing section. The behavioral
2 experiments, including the two-step task and the Balloon Analogue Risk task (BART)
3 were completed by all participants before MRI scanning. All participants were paid as
4 soon as they finished the MRI scanning procedure and dismissed. The study was
5 approved by the Institutional Review Board of Southwest University.

6 **2.2.1 Two-step task**

7 Daw and colleagues developed a two-step Markovian decision task and
8 computational model that estimates a parameter (the model-based weighting
9 parameter ω) which captures the balance between model-free versus model-based
10 learning (Daw et al., 2011; Daw et al., 2005; Doll et al., 2015; Gläscher et al., 2010;
11 Lee et al., 2014). For the current project, we used a modified version of this task that
12 incorporated changes proposed by Kool et al (2016), see also Lesage and Verguts
13 (2021). The task paradigm took about 25 minutes (depending on the participant's
14 response time). The task (illustrated in Figure 1) was embedded in a narrative where
15 the participants choose one of two animals as a guide to find a treasure chest. The
16 goal is to accumulate as many golden coins (points) as possible. Two animals were
17 presented at each trial; participants click "F" to choose the left one and "J" to choose
18 the right one. Each animal deterministically lead to one of two reward-dispensing
19 treasure chests; participants clicked the spacebar to open the treasure chest. The
20 reward dispensed by the treasure chest ranged from 0 to 10 golden coins and changed

1 across trials with the minimum change being 3 coins (for instance, if a participant
2 received 2 coins on a particular trial, then he or she would get at least 5 coins, a
3 number of coins that bigger than 5 but no more than 10, on the next trial when
4 choosing the equivalent animal). The two stimulus pairs presented to participants
5 were equivalent, such that stimuli A and C, and stimuli B and D always led to the
6 same treasure chest (see Figure 1). This task structure allows for separable responses
7 depending on whether a model-free or a model-based strategy is used. Animals A and
8 C always yielded the same outcome as animals B and D. The model-based system can
9 exploit this task structure to update the value of the stimuli: for example, when a
10 treasure chest linked to stimulus A suddenly yields a high point value, a model-based
11 learner can generalize this value update to stimulus C. By contrast, the model-free
12 system, which relies only on the learning history with the stimulus itself (C), could
13 not use the information obtained about the yoked stimulus A.



1 **Figure 1** Structure of the two-step task with deterministic transitions. The participants
 2 need to find treasure by choosing one of the two animals that would bring them to a
 3 treasure chest. The animals are linked in pairs: animals enclosed by solid circles
 4 would always receive the same value reward from the treasure chest; likewise for
 5 animals enclosed by dashed circles.

6

7 A Rescorla-Wagner update rule was used to model choices by the model-based
 8 and the model-free system (Rescorla & Wagner, 1972). The rule was fit to the
 9 participant's choice behaviour. We fit a total of eight models with different
 10 combinations of five parameters: the inverse temperature β , the model-based
 11 weighting parameter ω , the learning rate α , the response stickiness parameter ρ , and
 12 the stimulus stickiness parameter π . Each of the models is described in more detail
 13 below.

14 Each system separately updates the values for all four stimuli. Take trial t , where
 15 stimulus pair A-B was presented and stimulus A was selected. The model-free learner
 16 updates the model-free value of stimulus A ($V_{MF}(A_t)$) based on the previous model-
 17 free value of A ($V_{MF}(A_{t-1})$) and the outcome at trial t .

$$18 \quad V_{MF}(A_t) = V_{MF}(A_{t-1}) + \alpha * (V_{MF}(A_{t-1}) - \text{Outcome}_t)$$

19 The model-based learner similarly updates the model-based value of A based on
 20 the previous model-based value of A and the outcome.

$$21 \quad V_{MB}(A_t) = V_{MB}(A_{t-1}) + \alpha * (V_{MB}(A_{t-1}) - \text{Outcome}_t)$$

1 In addition, as the model-based learner is able to exploit the task structure (the
 2 equivalence between A and C), the model-based value of stimulus C is also updated
 3 to be the same as the model-based value of stimulus A.

4 $V_{MB}(C_t) = V_{MB}(A_t)$. A similar argument holds for stimulus pair B – D.

5 Values are weighted by model-based weighting parameter ω to arrive at the
 6 combined value for each stimulus. The weighting parameter ω ranges from 0 to 1,
 7 such that 0 indicates behaviour that is fully model-free, whereas 1 indicates behaviour
 8 that is fully model-based.

9
$$V(A_t) = \omega * V_{MB}(A_t) + (1 - \omega) * V_{MF}(A_t)$$

10 A softmax rule is used to compute the probability of the participant selecting
 11 stimulus A (out of a choice between A and B).

12 The β parameter is the inverse temperature parameter which captures the
 13 exploration-exploitation trade-off. The decisions of the participant become fully
 14 random (i.e., exploratory) when $\beta \rightarrow 0$. In contrast, when $\beta \rightarrow \infty$, participants fully
 15 exploit current knowledge about the task and choose the stimulus bearing the highest
 16 expected reward.

17 We included two additional parameters. One represents the participant's
 18 tendency to repeat responses (response stickiness parameter ρ), the other represents
 19 the tendency to repeat choices (stimulus stickiness parameter π ; Kool et al., 2016,
 20 2017). Thus, the softmax rule turns out as follows:

$$1 \quad P_t(A) = \frac{\exp(\beta * [V(A_t) + \pi * rep(A) + \rho * resp(A)])}{\exp(\beta * [V(A_t) + \pi * rep(A) + \rho * resp(A)]) + \exp(\beta * [V(B_t) + \pi * rep(B) + \rho * resp(B)])}$$

2 The variable $resp(A)$ indicates whether the position (i.e., left or right) of the
3 chosen response (button) is the same as the previously chosen response (button). The
4 response stickiness parameter ρ reflects how often the participant presses the same
5 button. Participants tend to repeat pressing the same button when $\rho > 0$, and switch to
6 another button when $\rho < 0$.

7 The variable $rep(A)$ indicates whether stimulus A is the same chosen stimulus in
8 the preceding trial. The stimulus stickiness parameter π reflects how consistently the
9 participant chooses the same stimulus between two successive trials. Participants are
10 inclined to choose the same stimulus when $\pi > 0$, and switch choices between two
11 consecutive trials when $\pi < 0$. The softmax rules are analogous for the other stimuli
12 (B, C, and D).

13 **2.2.2 Model Space**

14 We tested eight models with different parameters. Across the models we tested
15 different combinations of parameters including learning rate and stickiness
16 parameters. The models are detailed further in Table 1. Specifically, model 1 is a full
17 model with all 5 parameters (weighting parameter ω , inverse temperature parameter β ,
18 learning rate α , response stickiness parameter ρ , and stimulus stickiness parameter π).
19 Model 2 is a full model but without the stimulus stickiness parameter (4 parameters).
20 Model 3 is also a full model but without any stickiness parameters (3 parameters).

1 Model 4 includes both stickiness parameters with learning rate α set to 1 (4
2 parameters). Model 5 includes only the response stickiness parameter (learning rate α
3 = 1; 3 parameters at total). Model 6 excludes the stickiness parameters (learning rate
4 $\alpha=1$, 2 parameters at total). Model 7 is a full model but with two learning rates (there
5 is separate learning rate for model-based and model free, 6 parameters at total). Model
6 8 includes only the stimulus stickiness parameter (learning rate $\alpha=1$, 3 parameters at
7 total).

8 We chose to include model 4-6 in which learning rate was set to 1 (i.e., perfect
9 learning) because in version of the task we used, developed by Kool et al (2016), we
10 expected very high learning rates, higher than those previous found in other versions
11 of the two-step task. One reason was the reward presentation. We used a number of
12 reward points (golden coins) instead of fluctuating reward probabilities (for instance,
13 Gaussian drift). As a result, each choice had a specific outcome and reward was
14 completely reliable. A second reason was the adoption of deterministic rather than
15 probabilistic transitions in the present task. Since a high learning rate was expected
16 across participants, setting the learning rate 1 allowed us to better identify any roles of
17 the other parameters.

18 All models were compared by using random effects Bayesian model selection
19 (BMS, Stephan et al., 2009). We used the *mfit* toolbox
20 (<https://github.com/sjgershm/mfit>) running on MATLAB R2020b (The Math Works,
21 Inc., <http://www.mathworks.com/>). All free parameters within each model were

1 estimated for each participant individually using the maximum *a posteriori* (MAP)
2 estimate with empirical priors based on the approach taken in Gershman (2016). A
3 gamma distribution was employed as the prior distribution for the inverse
4 temperature. The lower and upper bounds of the inverse temperature were 0 and 50.
5 Both the balance parameter ω and learning rate parameter α had uniform priors
6 (specifically, prior distributions of equal probability with values that fell between the
7 boundaries 0 and 1). In addition, $\pi, \rho \sim (0.15, 1.42)$ were used as the prior distribution
8 of both stickiness parameters (with lower and upper bounds of -5 and 5). Finally, the
9 parameter with the maximum log-likelihood from the optimization process (10 times)
10 was selected. The winning model was identified according to the corresponding
11 protected exceedance probability (PXP) of each model as revealed by BMS. The PXP
12 protects against the null possibility which means that there are no potential differences
13 across different models. In addition, the PXP does not suffer from an overconfidence
14 bias in comparison with exceedance probability when conducting random effects
15 BMS (Rigoux et al., 2014).

16 **2.2.3 The Balloon Analogue Risk Task**

17 The Balloon Analogue Risk Task (BART) is a computer-based behavioral task
18 (Lejuez et al., 2002; Rao et al., 2008). The present study implemented this task using
19 the Psychtoolbox package under the environment of Matlab software. The goal of this
20 task for each participant is to earn as much money as they can by inflating a balloon

1 without bursting. The larger the balloon, the more the reward. The task in the present
2 study included 350 trials. For each trial, a blue balloon was presented in the center of
3 the screen. At the same time, two message boxes about reward were shown under the
4 balloon. One indicated the cumulative reward that the participant had earned thus far.
5 The other indicated the amount of reward earned on the immediately preceding trial.
6 Each of the inflations participants made could cause the balloon to grow larger
7 (accumulate ¥1 per pump, Yuan, RMB) or explode (loss the reward of that trial).
8 Participants could stop inflating the balloon and “cash out” at any time point during a
9 balloon. The probability of an explosion event was set as a monotonically increasing
10 function across trials: 0, 2.1%, 4.2%, 6.3%, 14.6%, 23.9%, 31.3%, 43.8%, 56.3%,
11 68.8%, 79.2%, 89.6% for smallest balloon to the largest balloon respectively. This
12 version of the BART differed from previous versions in that all the balloons had
13 equivalent explosion probabilities and were displayed in the same color (previous
14 versions used two or more algorithms, associated with different colors of balloons),
15 and participants completed a larger number of trials (previous versions typically were
16 performed for 40 trials (see Lejuez et al., 2002, for a description of the original BART
17 design). Participants were instructed to gain as much reward as possible and that each
18 burst balloon would result in nothing earned on that trial. Before the task, participants
19 were told to imagine the value of ¥1 to them in real life. Importantly, the algorithm
20 determining the explosion likelihood for each balloon was kept secret from the
21 participants. Participants were told that in addition to a base payment of ¥20 for their

1 participation, they could earn an additional bonus for good performance. This bonus
2 was calculated as the total number of points earned divided by 10. Participants could
3 earn up to ¥35 when the bonus was included.

4 The primary dependent measure was adjusted pumps, calculated as the average
5 number of inflation steps completed across intact balloon trials only (Lejuez et al.,
6 2002). Total amount of reward earned and the total number of balloons that burst
7 across the experiment were also calculated for each participant (McCormick & Telzer,
8 2017; Blair et al., 2018). Finally, the Coefficient of Variation of adjusted pumps
9 (COV) was also calculated for each participant. COV was defined as the standard
10 deviation of adjusted pumps divided by the average number of adjusted pumps (Blair
11 et al., 2018). The COV measures the consistency of performance across the whole
12 task, and has been shown to be an effective measure of individual variability
13 (DeMartini et al., 2014; Blair et al., 2018).

14 **2.3 fMRI Data Acquisition**

15 MRI data (structural and resting-state images) were acquired at Southwest
16 University with a TRIO 3.0T scanner (Siemens Magnetom Trio TIM, Erlangen,
17 Germany). All participants' high-resolution anatomical T1-weighted images were
18 collected through using the Magnetization Prepared Rapid Acquisition Gradient-Echo
19 (MPRAGE) sequence (repetition time (TR) = 2530 ms, echo time (TE) = 3.39 ms,
20 voxel size = $1 \times 1 \times 1.33$ mm³, slices = 128, flip angle (FA) = 7°; 256×256 matrix, last

1 for 3 min). Functional resting-state images were acquired using a T2*-weighted echo-
2 planar imaging sequence (TR = 2000 ms, FA = 90°, TE = 30 ms, resolution matrix =
3 64×64, FOV = 200×200 mm², voxel size = 3.1×3.1×3.6, 33 slices, 360 volumes, 12
4 min scanning). All participants were told to keep their eyes open, stay calm, and
5 refrain from excessive head motion (less than 1.5 mm).

6 **2.3.1 VBM analysis**

7 The VBM analysis was performed using Statistical Parametric Mapping
8 (SPM12) software (<http://www.fil.ion.ucl.ac.uk/spm/software/spm12/>)(accessed 13
9 February 2022).

10 **2.3.1.1 Preprocessing**

11 At the first step, individual high-resolution T1-weighted images were manually
12 adjusted to match the anterior-posterior commissures (AC-PC) line for each
13 participant. Subsequently, these T1-weighted structural images were segmented into
14 gray matter (GM), white matter (WM) and cerebral spinal fluid (CSF) by using the
15 segmentation tool of the toolbox. After that, flow fields and the group-specific
16 template was created for each participant using the DARTEL algorithm.
17 Normalization of GM images into Montreal Neurological Institute (MNI) space was
18 performed on the basis of this group-specific template. Finally, all the images were
19 modulated by using Jacobean determinants for the purpose of conserving the absolute

1 amount of GM and smoothed in order to improve signal-to-noise-ratio (8 mm, full
2 width at a half-maximum (FWHM) Gaussian kernel).

3 **2.3.1.2 Second Level Modeling Analysis**

4 In order to obtain cluster size for every individual, statistical modeling was
5 performed for all the GM images. We first executed multiple linear regression with
6 the model-based weighting parameter ω as the variable of interest within SPM12. A
7 MATLAB script “get_totals”
8 (http://www.cs.ucl.ac.uk/staff/g.ridgway/vbm/get_totals.m) (accessed 13 February
9 2022) was used to calculate the Global GM volume. Consistent with previous
10 studies, total GM volume, gender and age for each participant were set as
11 confounding variables inside the regression model (Goldstein et al., 2001; Barnes et
12 al., 2010; Callaert et al., 2014). In order to reduce the probability of false negatives,
13 an explicit mask was used rather than traditional absolute or relative threshold
14 masking through the population-specific masking toolbox implemented in SPM12
15 (Ridgway et al., 2009). Finally, T contrasts were examined to identify voxels which
16 had significant association with the weighting parameter ω . For brain areas where we
17 had *a priori* hypotheses about changes in gray matter volume (GM volume; i.e.,
18 cerebellum, caudate, dorsolateral prefrontal cortex, and inferior parietal lobule), small
19 volume correction (SVC: sphere with a 20 mm radius, threshold at $p < 0.05$) was used

1 for the VBM analyses. Multiple comparisons correction was performed using the
2 Family-Wise Error (FWE) method.

3 **2.3.2 rs-FC Analysis**

4 **2.3.2.1 Preprocessing**

5 All participants' resting-state functional images were preprocessing by the Data
6 Processing Assistant for Resting-State fMRI (DPARSF) software toolbox (Yan &
7 Zang, 2010) under the environment of MATLAB 2014b. The first 10 volumes of each
8 functional image were removed to allow the signal to reach equilibrium and to allow
9 participants to adapt to the scanning noise. Next, we performed Slice Time Correction
10 for temporal shifts and realigned (reference slice: middle image volume) to correct for
11 head motion. Then all participants' residual volumes were spatially normalized into
12 standard template, resampled (voxel sizes: $3 \times 3 \times 3 \text{ mm}^3$) and spatially smoothed (4
13 mm, FWHM). Linear detrending and bandpass temporal filtering at 0.01–0.08 Hz
14 were implemented for all participants' functional images. Friston-24 motion
15 parameters, white matter, CSF and global mean signal were regressed out from the
16 resting-state images to further reduce the effect of head motion and nuisance signals
17 (Saad et al., 2012). In addition, we performed framewise motion censoring to control
18 for head motion related artifacts. We removed volumes that exceeded a threshold of
19 0.2 mm frame-to-frame head motion displacement (FD). Specifically, if the FD value
20 of the volume being examined was greater than 0.2 mm then this volume was

1 excluded from the analysis along with the one preceding and two following volumes
2 (Power et al., 2012; Power et al., 2013) (the average number of excluded time points
3 across participants was 21, and no participants had greater than 50% of their time
4 points excluded).

5 **2.3.2.2 Functional Analysis**

6 Region-based functional connectivity analyses were implemented through the
7 Resting-State fMRI Data Analysis Toolkit V1.8 (REST) software package running on
8 MATLAB 2014 (Song et al., 2011). Regions of interest (ROI) were defined based on
9 the VBM results. Next, the Pearson's correlation coefficient was calculated between
10 the extracted average BOLD signal time course within each seed region and the time
11 course of every other voxel across the whole brain. The resulting correlation
12 functional connectivity (FC) maps were converted into normally distributed z -value
13 maps through Fisher z -transformation for further group-level analysis.

14 To further test whether the weighting parameter ω was correlated with functional
15 connectivity between the RCere and LIPL seed regions and other brain areas, a
16 Spearman's correlation analysis between ω and the above z -value maps was
17 performed. The thresholds for multiple comparisons correction were set at the voxel
18 level at $p < 0.005$ and at the cluster level at $p < 0.05$ (Gaussian random field (GRF)
19 theory, one-tailed, with a whole-brain mask, corrected). Areas that were significantly

1 correlated with the seed region and survived the multiple comparison correction were
2 saved as a mask for further analysis.

3 For the purpose of evaluating if there were any associations between the
4 functional connectivity networks identified above and risk-taking, we performed
5 correlation and mediation analyses. The connectivity value obtained from the ROI
6 seed FC maps was extracted and converted using Fisher's z transform. Next, we
7 performed a Pearson's correlation analysis between this converted connectivity value
8 and participants' risk-taking measure (mean adjusted pumps on the BART). Finally,
9 Hayes's (2009) PROCESS macro (INDIRECT procedure in SPSS) was employed to
10 estimate the mediation model (95% confidence level, 5000 bootstrap samples; Hayes,
11 2009). During this analysis procedure, direct effects (the effect of independent
12 variable on dependent variable after controlling the effect of mediator, path c'),
13 indirect effects (the effect of the independent variable on the mediator and the effect
14 of the mediator on the dependent variable, i.e., path ab) and total effects (the effect of
15 independent variable on dependent variable, path c) were extracted. It was important
16 to assess the indirect effects (path ab) of the independent variable on the dependent
17 variable. A significant indirect effect exists when the zero is not included within the
18 bias-corrected bootstrap-confidence (CI).

19 **3 Results**

20 **3.1 Bayesian model comparison and selection**

1 All eight models (see Table 1) were fit individually to each of the subjects. Then
 2 we applied Bayesian model comparisons to select the winning model, defined as the
 3 one that showed the highest score of PXP. The model comparison results revealed that
 4 Model 4 (which included 4 free parameters: the weighting parameter ω , inverse
 5 temperature parameter β , the response stickiness parameter ρ ; and the stimulus
 6 stickiness parameter π , and which had learning rate α set to a constant value of 1) was
 7 the winning model and was clearly superior to the other seven alternative models (see
 8 Table 1). Subsequently, all following analyses were based on the results of Model 4.

9 **Table 1** Two-Step Task Parameter estimate

	Model1	Model2	Model3	Model4	Model5	Model6	Model7	Model8
	$(\omega, \beta, \alpha,$ $\rho, \pi)$	$(\omega, \beta, \alpha,$ $\rho)$	$(\omega, \beta,$ $\alpha)$	$(\omega, \beta, \rho,$ $\pi, \alpha=1)$	$(\omega, \beta, \rho,$ $\alpha=1)$	$(\omega, \beta,$ $\alpha=1)$	$(\omega, \beta, \rho,$ $\pi, 2\alpha)$	$(\omega, \beta, \pi,$ $\alpha=1)$
EXP	0.010	0.005	0.005	0.959	0.005	0.005	0.005	0.005
XP	0.000	0.000	0.000	1.000	0.000	0.000	0.000	0.000
PXP	0.000	0.000	0.000	1.000	0.000	0.000	0.000	0.000

10 Note. EXP: expected posterior probabilities; XP: exceedance probabilities; PXP:
 11 protected exceedance probabilities. ω : the weighting parameter; β : the inverse
 12 temperature parameter; α : learning rate; ρ : response stickiness parameter; π : stimulus
 13 stickiness parameter.

14 3.2 Behavioral Results

1 Behavioral results from the two-step task and the BART are shown in Tables 2
2 and 3, respectively. We used the weighting parameter ω from the two-step task and
3 the mean adjusted pumps from the BART task as our primary dependent measures.
4 We first carried out a Kolmogorov-Smirnov test which found that the mean adjusted
5 pumps from the BART was normally distributed in our sample, but the weighting
6 parameter ω from the two-step task was not (weighting parameter ω , Kolmogorov-
7 Smirnov $z = 2.858, p < 0.05$; Risk-taking: Kolmogorov-Smirnov $z = 0.653, p > 0.05$).
8 Therefore, we performed a Spearman's correlation analysis (which is appropriate for
9 non-normally distributed data) which indicated that weighting parameter ω was
10 positively correlated with risk-taking as measured by mean adjusted pumps ($r =$
11 $0.170, p < 0.05$; see Figure 2). For the COV, a measure of consistency, the weighting
12 parameter ω was negatively correlated ($r = -0.151, p < 0.05$).

13 We also examined whether there were age or gender effects on the behavioural
14 tasks. Neither the correlation between age and weighting parameter ω ($r = -0.041, p >$
15 0.05), nor that between age and BART mean adjusted pumps ($r = 0.077, p > 0.05$)
16 were significant. Finally, t-tests indicated no gender differences in the weighting
17 parameter ω (t (df =189) = 1.100, $p > 0.05$), or in BART mean adjusted pumps (t (df
18 =189) = 1.748, $p > 0.05$).

19

20

1 **Table 2** Two-Step Task Parameter estimates

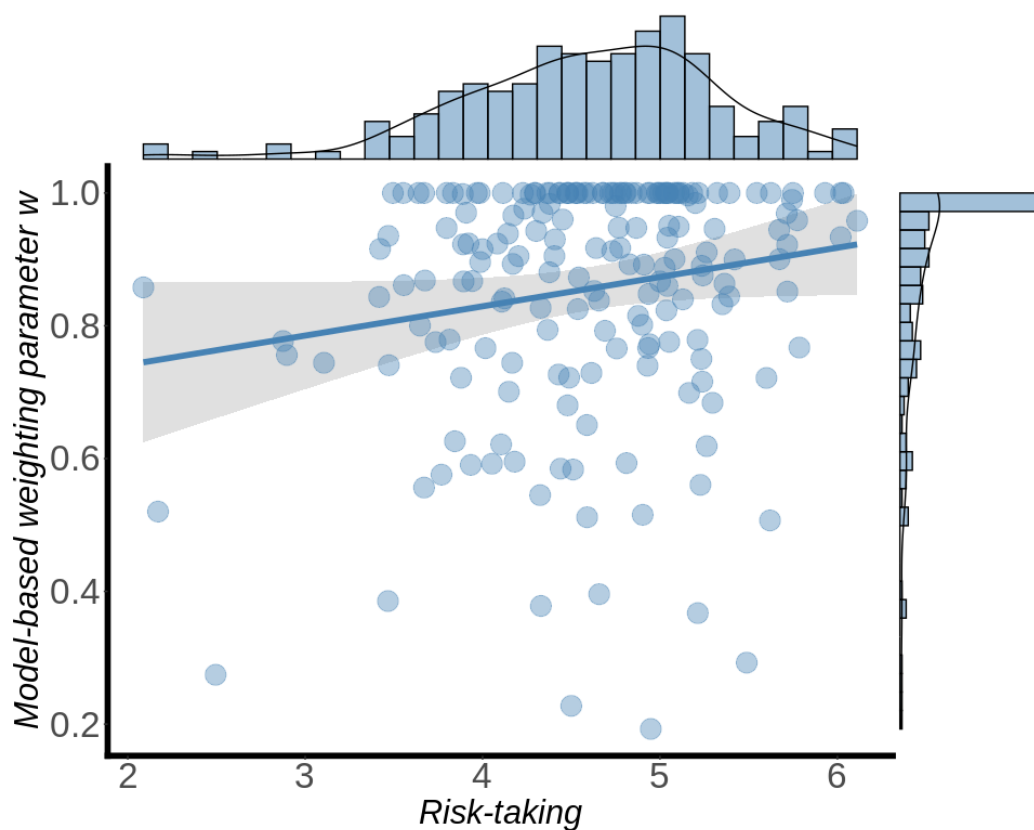
Predictor	ω	β	α	ρ	π
25th percentile	0.78	3.00	1.00	1.00	1.46
Median	0.92	4.00	1.00	1.00	1.65
75th percentile	1.00	5.00	1.00	2.00	1.88

2 Note. ω : the weighting parameter; β : the inverse temperature parameter; α : learning
 3 rate; ρ : response stickiness parameter; π : stimulus stickiness parameter.

4 **Table 3** BART Descriptive Statistics

	Mean (Standard Deviation)
BART Performance	
Mean Adjusted Pumps	4.57 (0.74)
Total Points Earned	215.07 (22.15)
Total Explosions	300.96 (13.06)
COV-All participants	0.22 (0.07)

5 Note. BART: Balloon Analogue Risk Task; COV: Coefficient of Variation of adjusted
 6 pumps during BART; ω : the model-based weighting parameter of two-step task.



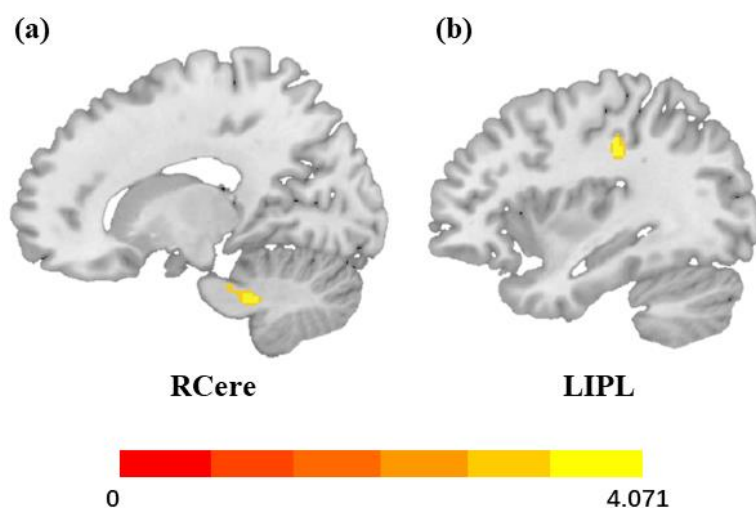
1

2 **Figure 2** Behavioral results (191 participants). Bottom left panel: Scatterplot of
 3 model-based weighting parameter (ω) and the risk-taking scores (mean adjusted
 4 pumps) on the BART. The weighting parameter ω was significantly positively
 5 correlated with risk-taking ($r = 0.170$, $p < 0.05$). Top panel: Histogram of risk-taking
 6 scores. Right panel: Histogram of the weighting parameter ω .

7 **3.3 VBM Neuroanatomical Results**

8 The weighting parameter ω was positively correlated with GM volumes in two
 9 of the hypothesized areas, as shown in Figure 3. These regions were the right
 10 cerebellum (RCere; MNI center coordinates: 15, -39, -36; Cluster size = 170 voxels;
 11 SVC-based $p_{\text{FWE-corr}}=0.025$, SVC corrected), and left inferior parietal lobule (LIPL;

- 1 MNI center coordinates: -36, -25.5, 34.5; Cluster size = 232 voxels; SVC-based $p_{\text{FWE-corr}}=0.015$, SVC corrected).
- 2 $p_{\text{FWE-corr}}=0.015$, SVC corrected).



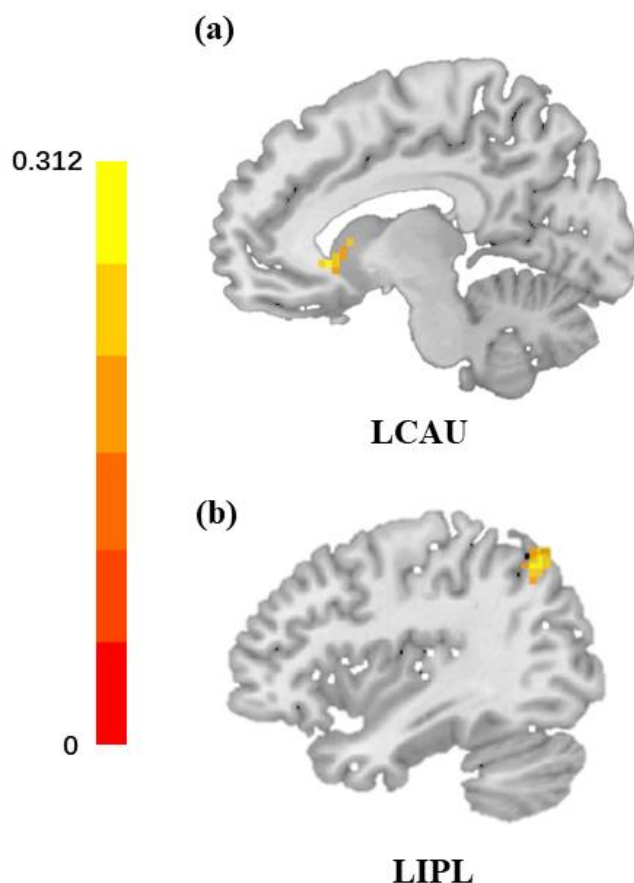
- 3
- 4 **Figure 3** VBM results for model-based learning. The GM volumes in (a) the right
- 5 cerebellum (RCere; MNI center coordinates: 15, -39, -36; Cluster size = 170 voxels;
- 6 SVC-based $p_{\text{FWE-corr}}=0.025$, SVC corrected), and (b) left inferior parietal lobule
- 7 (LIPL; MNI center coordinates: -36, -25.5, 34.5; Cluster size = 232 voxels; SVC-
- 8 based $p_{\text{FWE-corr}}=0.015$, SVC corrected) were positively correlated with the model-
- 9 based weighting parameter ω .

10 3.4 Resting-state Functional Connectivity Results

- 11 The two ROIs identified in the VBM analysis were used as seed regions in the
- 12 functional connectivity analyses following the procedures outlined in the Methods
- 13 section for each of the ROIs. The specific ROIs were formed as 9 mm spheres
- 14 surrounding the center voxel of the cluster identified in the VMB analysis (RCere: $x =$

1 15, $y = -39$, $z = -36$; LIPL: $x = -36$, $y = -25.5$, $z = 34.5$) following the procedures
2 established in previous research (Fang et al., 2019; Zhou et al., 2019; Benetti et al.,
3 2021). We then applied a Spearman's correlation analysis to evaluate whether the
4 weighting parameter ω was correlated with the functional connectivity networks. ω
5 was positively correlated with functional connectivity between the RCere seed region
6 and two other regions illustrated in Figure 4: the left caudate (LCAU; MNI peak
7 coordinates: -9, 24, -3; cluster size = 79; $r = 0.264$, voxel significance: $p < 0.005$;
8 cluster significance: $p < 0.05$, GRF corrected), and the left inferior parietal lobule
9 (LIPL, MNI peak coordinates: -39, -66, 51; cluster size = 68; $r = 0.312$, voxel
10 significance: $p < 0.005$; cluster significance: $p < 0.05$, GRF corrected; see Figure 4).
11 No significant relationship was found between ω and connectivity between the LIPL
12 seed and other brain regions.

13 A second analysis examined the correlation between risk-taking (mean adjusted
14 pumps in the BART) and the two functional connectivity patterns identified as
15 correlating with ω (RCere- LCAU and RCere- LIPL). Connectivity between RCere-
16 LCAU was positively correlated with risk-taking ($r = 0.206$, $p < 0.01$). However,
17 functional connectivity between RCere- LIPL was not significantly correlated with
18 risk-taking ($r = -0.024$, $p > 0.05$).



1

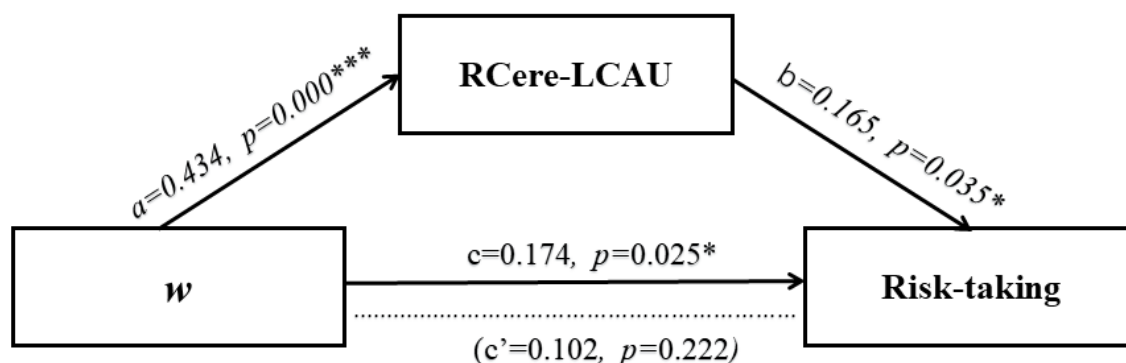
2 **Figure 4** Resting-state functional connectivity results between the right cerebellum
 3 (RCere) seed region of interest identified in the present VBM analysis and other brain
 4 areas that correlated with the weighting parameter ω . Functional connectivity between
 5 seed ROIs and left caudate (LCAU) (a) and left inferior parietal lobule (LIPL) (b)
 6 were both positively correlated with the weighting parameter ω (voxel significance: p
 7 < 0.005 , cluster significance: $p < 0.05$, GRF corrected).

8 **3.5 Mediation Analysis Results**

9 In order to test different theories of how functional connectivity in the RCere-
 10 LCAU system is related to model-based learning and risk taking we performed two
 11 mediation models. In the first model (mediation model 1), the independent variable

1 was the weighting parameter ω , the dependent variable was risk-taking, and the
2 mediator was the functional coupling between RCere-LCAU. In the second model
3 (mediation model 2), the dependent variable was risk-taking, the independent variable
4 was RCere-LCAU connectivity, and the mediator variable was model-based learning.
5 For both mediation analyses, the paths between the independent variable, dependent
6 variables, and mediator were estimated by using the INDIRECT procedure in SPSS
7 (Hayes, 2009; Preacher & Hayes, 2008). We found that mediation model 1 (Figure 5)
8 provided a good fit for the data: functional connectivity between RCere- LCAU
9 completely mediated the relationship between the weighting parameter ω and risk-
10 taking (95% percentile CI = 0.0053 to 0.1506, $p < .05$). We further examined whether
11 the model could generalize to new data by performing a 5-fold cross-validation
12 procedure using the scikit-learn python toolbox ([https://scikit-](https://scikit-learn.org/stable/index.html)
13 [learn.org/stable/index.html](https://scikit-learn.org/stable/index.html)). We found that model 1 yielded an average mean square
14 error (MSE) of 0.757, which means that model 1 generalized well to new data (Song
15 et al., 2021). In contrast, mediation model 2 did not successfully fit the data (95%
16 percentile CI = -0.0374 to 0.1178, $p > 0.05$). These two analyses indicate that the
17 relationship between model-based learning and risk-taking relies on the functional
18 connectivity between RCere-LCAU (as in mediation model 1), rather than the RCere-
19 LCAU connectivity having an influence on model-based learning that in turn
20 influences risk taking (as in mediation model 2). In order to ensure that the successful
21 mediation in model 1 was not influenced by potential effects of age, gender and mean

1 FD, we repeated the mediation controlling for age, gender and mean FD and found
 2 similar results to the original analysis (95% percentile CI=0.0188 to 0.1611, $p < .05$).



3

4 **Figure 5** Mediation results. The effect of the weighting parameter ω on risk-taking
 5 (measured by BART) was completely mediated by the association between right
 6 cerebellum (RCere) connectivity with the left caudate (LCAU). *: $p < 0.05$; ** $p <$
 7 0.01; ***: $p < 0.001$

8 **4 Discussion**

9 The present study investigated the relationship between model-based learning
 10 and risk taking using VBM analysis and rsFC and revealed several notable results.
 11 The model-based weighting parameter ω was positively correlated with risk taking on
 12 the BART. The VBM analysis identified the right cerebellum and left inferior parietal
 13 lobe as anatomical correlates of model-based learning. Functional connectivity results
 14 revealed that functional coupling between the right cerebellum and the left caudate
 15 was positively correlated with both the weighting parameter ω and risk taking.

1 Finally, mediation analysis found that functional connectivity between the right
2 cerebellum and the left caudate completely mediated the effect of weighting
3 parameter ω on risk taking.

4 Model-based reasoning was positively correlated with risk taking. Participants
5 with higher reliance on model-based learning made more inflationary pumps (higher
6 adjusted pump score), had a greater number of balloon bursts, and tended towards
7 more consistent strategy use (lower coefficient of variation). Model-based learning is
8 a computationally demanding process, but it enables individuals to respond precisely
9 and flexibly to a dynamic environment. These behavioral results support our
10 hypothesis that stronger executive functions may allow individuals to use a more
11 accurate, refined and sophisticated decision-making processes when making risky
12 decisions. The results are consistent with previous findings (Blair et al. 2018; Ogilvie
13 et al., 2020) which found that better performance on BART was associated with more
14 developed executive functions (but note also Kóbor et al (2015) suggested that
15 superior EFs might not be needed for optimal BART performance).

16 We should note that overall participants in our study were risk-averse, with the
17 average participant having a mean adjusted pumps of 4.57, whereas the optimal
18 stopping point for maximizing reward is higher. Thus, higher risk taking was
19 associated with better performance, consistent with our argument above that stronger
20 executive functions allowed participants to make better decisions. However, the
21 specific relationship between risk taking and performance depends on the task and

1 context of behavior, and in many circumstances high levels of risk-taking can lead to
2 decision making impairments when choosing high risk but unlikely options. Some
3 previous studies have found that individuals with high executive functions show a risk
4 aversive response in certain contexts (Fecteau et al., 2007).

5 We should also note that the task we used had several differences from the
6 original Daw et al task. Kool et al (2016) argued that the probability of getting a
7 binary reward in the original two-step task was not very informative and thus reduced
8 the accuracy of model-based learning system. Therefore, they modified the task to
9 include a fluctuating number of reward points (golden coins) and a deterministic
10 transitions structure (choice of the first-step stage leads to the same second-step
11 stage). These changes greatly increased the accuracy of model-based learning,
12 consistent with our results that a high learning rate fitted the data.

13 An improved understanding of the relation between risk and executive function
14 may help to understand how executive function relates to other constructs as well. For
15 example, risk taking has often been correlated with sensation seeking (the chase of
16 novel and exciting experiences) but sensation seeking itself is not accompanied by
17 executive function impairments (Romer et al., 2011).

18 Our results indicated an important role of the cerebellum in model-based
19 learning and risk taking. First, we found that gray matter volume in the right
20 cerebellum was positively correlated with ω . Second, we found that functional
21 connectivity between right cerebellum and the left caudate correlated with both ω and

1 risk-taking. The cerebellum is an important component of the frontal cortical-basal
2 ganglia-cerebellum circuits that are critical in mediating motivation, planning,
3 working memory, cognitive control and motion preparation (Stoodley et al., 2010;
4 Hampshire et al., 2010; Behan et al., 2015; Doll et al., 2015; Lemire-Rodger et al.,
5 2019; Huo et al., 2020; Dong et al., 2022). Patients with cerebellar lesions engage in
6 more risky decisions (Miquel et al., 2016; Berg et al., 2020). Cardoso et al (2014)
7 found that patients with cerebellar strokes displayed impaired performance on the
8 Iowa Gambling Task (IGT), selecting fewer advantage decks, as compared with
9 healthy controls. This suggests an active role of cerebellum in decision-making, an
10 important component of EFs. Previous research found that bilateral gray matter
11 volume of Crus 1 region of cerebellum was positively associated with novelty
12 seeking, a personality trait that correlates with risk-taking (Petrosini et al., 2015;
13 Laricchiuta et al., 2013). Quan et al (2022) reported a strong positive association
14 between gray matter volume (GMV) of left cerebellum with participants' risk-taking
15 behavior and risk tolerance. Furthermore, left cerebellum GMV also statistically
16 mediated risk-taking behavior and risk tolerance changes with aging (Quan et al.,
17 2022). Aydogan et al (2021) found that higher cerebellum GMV was associated with
18 improved optimal decision making and decreased tendencies toward suboptimal risky
19 behavior. The cerebellum may support model-based reasoning through its
20 computational process of error correction based on forward models, which may be

1 used to predict the outcomes of ambiguous events of the environment and learn from
2 feedback (Imamizu & Kawato, 2009; Blackwood et al., 2004).

3 We also found an important role for the caudate nucleus and functional
4 connectivity between the caudate and cerebellum. Our functional connectivity
5 analyses revealed that connectivity between the right cerebellum seed and left caudate
6 was significantly correlated with both model-based reasoning and risk-taking.
7 Furthermore, the mediation analysis showed that the right cerebellum and the left
8 caudate coupling completely mediated the effect of the weighting parameter ω on
9 risk-taking. The role of the caudate in model-based reasoning is supported by a recent
10 meta-analysis (Huang et al., 2020) finding greater dorsal caudate activity in trials
11 driven by model-based processes in contrast with trials driven by model-free
12 processes. It is also consistent with a resting state fMRI study that found differences
13 in the caudate at rest that correlated with model-based reasoning (Gentili et al., 2022).
14 These results are further consistent with the role of the caudate in goal-directed
15 instrumental learning more broadly (Seger, 2018). Recent research has established
16 that there is pervasive functional and anatomical connectivity between the caudate
17 and cerebellum (Bostan et al., 2013; Bostan & Strick, 2018). Sang et al (2012) found
18 that both the sensorimotor and cognitive related cerebellar subregions (lobules V, VII
19 and VIII) were correlated with the basal ganglia in rsFC analyses. Interactions
20 between basal ganglia and cerebellum are essential for learning, planning and control
21 processes (Nambu, 2008; Bostan & Strick, 2018). The interactions inside basal

1 ganglia–cerebellar–cerebral cortical networks are important for both reward-based
2 and error-based learning (Jueptner et al., 1997; Li et al., 2012; Bornstein et al., 2013).

3 Finally, we found a role for the lateral parietal cortex: gray matter volume in the
4 LIPL was associated with model-based reasoning. This result is consistent with
5 findings that differences in the ALFF signal in the IPL at rest correlate with model-
6 based reasoning (Gentili et al., 2022). The parietal cortex is known to participate in
7 the frontoparietal multiple demand system and play an important role in attentional
8 processes (Corbetta & Shulman, 2002; Zwosta et al., 2018). One potential role of the
9 parietal lobe is as part of an episodic memory system that may be important in model-
10 based reasoning (Bornstein et al., 2013; Stoianov et al., 2018). In model-based
11 reinforcement learning, participants expect and memorize the future states of
12 consequences according to their relevant choices. Significantly, inferior parietal
13 lobule, cuneus, lingual gyri and hippocampus are essential regions of the memory
14 network in encoding and retrieving motion or behavioral events (Addis et al., 2009;
15 Schacter et al., 2012). Furthermore, the bilateral parietal visuospatial system has been
16 associated with reasoning about unfamiliar situations (Goel et al., 2000; Goel &
17 Dolan, 2003), consistent with the reasoning demands of the two-step task.

18 The current study has several limitations. First, the experimental method used
19 were correlational and thus could not establish causality or rule out competing neural
20 mechanisms. To address this, future studies could combine well design experimental
21 task with causal methods. For example, brain stimulation technology (e.g., high

1 precision transcranial direct current stimulation (tDCS)) could be adopted in future
2 research to explore causality. It would be worthwhile to test whether model-based
3 learning could be changed by stimulating certain brain areas via tDCS and if this
4 intervention would have a beneficial effect on individuals with excessively high or
5 low risk-taking tendencies. Although our present study has a large sample size when
6 compared with the relatively low median sample size of imaging studies in the field, it
7 still may be insufficient. Marek et al (2022) recently argued that it is necessary to
8 have sample sizes in the thousands to have accurate effect size estimations and high
9 replication rates in brain-wide association studies (BWAS). Thus, future research
10 should recruit larger participant samples to achieve more robust BWAS effects.
11 Lastly, a relatively lenient threshold for multiple comparisons correction was adopted
12 in present study. Thus, this study should be considered to be exploratory and should
13 be replicated in future research.

14 In conclusion, these results suggest that model-based learners engage in more
15 risky behaviors through interactions between reward-based learning, error-based
16 learning and episode future thinking subserved by basal ganglia, cerebellum and
17 inferior parietal lobule.

18

1 **Credit authorship contribution statement**

2 Hangfeng Huo: Design, data collection, Methodology, Software, Formal analysis,
3 Data curation, Writing - original draft, Writing - review & editing. Elise Lesage:
4 Investigation, Methodology, Software, Formal analysis. Wenshan Dong:
5 Methodology, Formal analysis. Tom Verguts: Investigation, Methodology, Writing -
6 review & editing. Carol A. Seger: Methodology, Writing - review & editing,
7 Validation. Sitong Diao: Formal analysis. Tingyong Feng: Conceptualization,
8 Methodology, Project administration, Validation. Qi Chen: Conceptualization,
9 Methodology, Project administration, Supervision, Writing - review & editing,
10 Validation, Funding acquisition

11

12 **Funding**

13 This work was supported by National Natural Science Foundation of China (Grant
14 No. 32071049), National Science and Technology Innovation 2030 Major Program
15 (Grant No. 2021ZD0203800), Guangdong Basic and Applied Basic Research
16 Foundation, China (No. 2022A1515012185), and the Neuroeconomics Laboratory of
17 Guangzhou Huashang College (No. 2021WSYS002).

18

19 **Conflict of interest**

20 None declared.

21

1 **Ethics statement**

2 The authors claim that all procedures in the current study comply with the ethical
3 standards of the national and institutional committees on human experimentation.

4

5 **Consent to participation**

6 All participants have given written informed consent before the experiment.

Reference

- Addis, D. R., Ling, P., Vu, M. A., Laiser, N., & Schacter, D. L. (2009). Constructive episodic simulation of the future and the past: distinct subsystems of a core brain network mediate imagining and remembering. *Neuropsychologia*, 47(11), 2222-2238.
- Aydogan, G., Daviet, R., Karlsson Linnér, R., Hare, T. A., Kable, J. W., Kranzler, H. R., ... & Nave, G. (2021). Genetic underpinnings of risky behaviour relate to altered neuroanatomy. *Nature Human Behaviour*, 5(6), 787-794.
- Barnes, J., Ridgway, G. R., Bartlett, J., Henley, S. M., Lehmann, M., Hobbs, N., Clarkson, M. J., MacManus, D. G., Ourselin, S., & Fox, N. C. (2010). Head size, age and gender adjustment in MRI studies: a necessary nuisance? *NeuroImage*, 53, 1244-1255.
- Behan, B., Stone, A., & Garavan, H. (2015). Right prefrontal and ventral striatum interactions underlying impulsive choice and impulsive responding. *Human Brain Mapping*, 36(1), 187.
- Benetti, S., Zonca, J., Ferrari, A., Rezk, M., Rabini, G., & Collignon, O. (2021). Visual motion processing recruits regions selective for auditory motion in early deaf individuals. *NeuroImage*, 230, 117816.
- Berg, N., Huitema, R. B., Spikman, J. M., Luijckx, G. J., & Haan, E. (2020). Impairments in emotion recognition and risk-taking behavior after isolated, cerebellar stroke. *The Cerebellum*, 19(1).

- Blackwood, N., Simmons, A., Bental, R., Murray, R., & Howard, R. (2004). The cerebellum and decision making under uncertainty. *Cognitive Brain Research*, 20(1), 46-53.
- Blair, M. A., Moyett, A., Bato, A. A., DeRosse, P., & Karlsgodt, K. H. (2018). The role of executive function in adolescent adaptive risk-taking on the balloon analogue risk task. *Developmental Neuropsychology*, 43(7), 566-580.
- Bleichrodt, H., L'Haridon, O., & Van Ass, D. (2018). The risk attitudes of professional athletes: Optimism and success are related. *Decision*, 5(2), 95.
- Bornstein, A. M., Daw, N. D., & Behrens, T. (2013). Cortical and hippocampal correlates of deliberation during model-based decisions for rewards in humans. *PLoS Computational Biology*, 9(12), e1003387.
- Bostan, A. C., Dum, R. P., & Strick, P. L. (2013). Cerebellar networks with the cerebral cortex and basal ganglia. *Trends in Cognitive Sciences*, 17(5), 241-254.
- Bostan, A. C., & Strick, P. L. (2018). The basal ganglia and the cerebellum: nodes in an integrated network. *Nature Reviews Neuroscience*, 19(Suppl. 3), 1-11.
- Braunlich, K., & Seger, C. (2013). The basal ganglia. *Wiley Interdisciplinary Reviews: Cognitive Science*, 4(2), 135-148.
- Brymer, E., & Schweitzer, R. (2013). Extreme sports are good for your health: a phenomenological understanding of fear and anxiety in extreme sport. *Journal of Health Psychology*, 18(4), 477-487.

Buckner, R. L. (2013). The Cerebellum and Cognitive Function: 25 Years of Insight from Anatomy and Neuroimaging. *Neuron*, 80, 807–815.

Castañeda, L. E. G., Sklarek, B., Dal Mas, D. E., & Knauff, M. (2023). Probabilistic and deductive reasoning in the human brain. *NeuroImage*, 275, 120180.

Callaert, D. V., Ribbens, A., Maes, F., Swinnen, S. P., & Wenderoth, N. (2014). Assessing age-related gray matter decline with voxel-based morphometry depends significantly on segmentation and normalization procedures. *Frontiers in Aging Neuroscience*, 6, 124.

Caulfield, M. D., Zhu, D. C., McAuley, J. D., & Servatius, R. J. (2016). Individual differences in resting-state functional connectivity with the executive network: support for a cerebellar role in anxiety vulnerability. *Brain Structure and Function*, 221(6), 3081-3093.

Choi, E. Y., Yeo, B. T., & Buckner, R. L. (2012). The organization of the human striatum estimated by intrinsic functional connectivity. *Journal of Neurophysiology*, 108(8), 2242-2263.

Corbetta, M., & Shulman, G. L. (2002). Control of goal-directed and stimulus-driven attention in the brain. *Nature Reviews Neuroscience*, 3(3), 201-215.

Crittenden, B. M., Mitchell, D. J., & Duncan, J. (2016). Task Encoding across the Multiple Demand Cortex Is Consistent with a Frontoparietal and Cingulo-Opercular Dual Networks Distinction. *Journal of Neuroscience*, 36, 6147–6155.

Daw, N. D., Gershman, S. J., Seymour, B., Dayan, P., & Dolan, R. J. (2011). Model-based influences on humans' choices and striatal prediction errors. *Neuron*, 69(6), 1204-1215.

Daw, N. D., Niv, Y., & Dayan, P. (2005). Uncertainty-based competition between prefrontal and dorsolateral striatal systems for behavioral control. *Nature Neuroscience*, 8(12), 1704-1711.

Dayan, P., & Niv, Y. (2008). Reinforcement learning: the good, the bad and the ugly. *Current Opinion in Neurobiology*, 18(2), 185-196.

Decker, S.L., Hill, S.K., Dean, R.S. (2007). Evidence of construct similarity in executive functions and fluid reasoning abilities. *International Journal of Neuroscience*, 117 (6), 735–748.

DeMartini, K. S., Leeman, R. F., Corbin, W. R., Toll, B. A., Fucito, L. M., Lejuez, C. W., & O'Malley, S. S. (2014). A new look at risk-taking: Using a translational approach to examine risk-taking behavior on the balloon analogue risk task. *Experimental and Clinical Psychopharmacology*, 22(5), 444.

Derefinko, K. J., Peters, J. R., Eisenlohr-Moul, T. A., Walsh, E. C., Adams, Z. W., & Lynam, D. R. (2014). Relations between trait impulsivity, behavioral impulsivity, physiological arousal, and risky sexual behavior among young men. *Archives of Sexual Behavior*, 43, 1149-1158.

Deserno, L., Wilbertz, T., Reiter, A., Horstmann, A., Neumann, J., Villringer, A., Heinze, H. J., & Schlagenhauf, F. (2015). Lateral prefrontal model-based

signatures are reduced in healthy individuals with high trait impulsivity.

Translational Psychiatry, 5(10), e659–e659.

D'Esposito, M., & Postle, B. R. (2015). The cognitive neuroscience of working memory. *Annual Review of Psychology*, 66, 115-142.

Doll, B. B., Duncan, K. D., Simon, D. A., Shohamy, D., & Daw, N. D. (2015).

Model-based choices involve prospective neural activity. *Nature*

Neuroscience, 18(5), 767-772.

Dong, W., Luo, J., Huo, H., Seger, C. A., & Chen, Q. (2022). Frontostriatal

Functional Connectivity Underlies the Association between Punishment

Sensitivity and Procrastination. *Brain Sciences*, 12(9), 1163.

Doya, K. (2000). Complementary roles of basal ganglia and cerebellum in learning and motor control. *Current Opinion in Neurobiology*, 10(6), 732-739.

Doya, K. (1999). What are the computations of the cerebellum, the basal ganglia and the cerebral cortex? *Neural Networks*, 12(7-8), 961-974.

Doya, K., Kimura, H., & Kawato, M. (2001). Neural mechanisms of learning and control. *IEEE Control Systems Magazine*, 21(4), 42-54.

Duncan, J. (2010). The multiple-demand (MD) system of the primate brain: mental programs for intelligent behaviour. *Trends in Cognitive Sciences*, 14(4), 172-179.

- Economides, M., Kurth-Nelson, Z., Lübbert, A., Guitart-Masip, M., & Dolan, R. J. (2015). Model-based reasoning in humans becomes automatic with training. *PLoS Computational Biology*, 11(9), e1004463.
- Ernst, M., & Paulus, M. P. (2005). Neurobiology of decision making: a selective review from a neurocognitive and clinical perspective. *Biological Psychiatry*, 58(8), 597-604.
- Fang, M., Aglinskas, A., Li, Y., & Anzellotti, S. (2019). Identifying hubs that integrate responses across multiple category-selective regions. *PsyArXiv*, November.
- Fecteau, S., Pascual-Leone, A., Zald, D. H., Liguori, P., Théoret, H., Boggio, P. S., & Fregni, F. (2007). Activation of prefrontal cortex by transcranial direct current stimulation reduces appetite for risk during ambiguous decision making. *Journal of Neuroscience*, 27(23), 6212-6218.
- Gentili, C., Di Rosa, E., Podina, I., Popita, R., Voinescu, B., & David, D. (2022). Resting state predicts neural activity during reward-guided decision making: An fMRI study on Balloon Analogue Risk Task. *Behavioural Brain Research*, 417, 113616.
- Gershman, S. J. (2016). Empirical priors for reinforcement learning models. *Journal of Mathematical Psychology*, 71, 1–6.
- Gläscher, Daw, N., Dayan, P., & O'Doherty, J. P. (2010). States versus rewards: dissociable neural prediction error signals underlying model-based and model-free reinforcement learning. *Neuron*, 66(4), 585-595.

- Goel, V., Buchel, C., Frith, C., & Dolan, R. J. (2000). Dissociation of mechanisms underlying syllogistic reasoning. *NeuroImage*, 12(5), 504-514.
- Goel, V., & Dolan, R. J. (2003). Explaining modulation of reasoning by belief. *Cognition*, 87(1), B11-B22.
- Goldstein, J. M., Seidman, L. J., Horton, N. J., Makris, N., Kennedy, D. N., Caviness Jr, V. S., Faraone, S. V., & Tsuang, M. T. (2001). Normal sexual dimorphism of the adult human brain assessed by in vivo magnetic resonance imaging. *Cerebral Cortex*, 11, 490-497.
- Habas, C., Kamdar, N., Nguyen, D., Prater, K., Beckmann, C. F., Menon, V., & Greicius, M. D. (2009). Distinct cerebellar contributions to intrinsic connectivity networks. *Journal of Neuroscience*, 29(26), 8586-8594.
- Hampshire, A., Chamberlain, S. R., Monti, M. M., Duncan, J., & Owen, A. M. (2010). The role of the right inferior frontal gyrus: inhibition and attentional control. *NeuroImage*, 50(3), 1313-1319.
- Hayes, A. F. (2009). Beyond Baron and Kenny: Statistical Mediation Analysis in the New Millennium. *Communication Monographs*, 76(4), 408-420.
- Huang, Y., Yaple, Z. A., & Yu, R. (2020). Goal-oriented and habitual decisions: neural signatures of model-based and model-free learning. *NeuroImage*, 215, 116834.
- Huo, H., Seger, C. A., Zhou, D., Chen, Z., Xu, T., Zhang, R., ... Chen, Q. (2020). The assessment dimension of regulatory mode mediates the relation between

- frontoparietal connectivity and risk-taking: Evidence from voxel-base morphometry and functional connectivity analysis. *Brain and Cognition*, 140, 105533.
- Huo, H., Zhang, R., Seger, C. A., Feng, T., & Chen, Q. (2020). The effect of trait anxiety on risk-taking: Functional coupling between right hippocampus and left insula. *Psychophysiology*, 57(10), e13629.
- Ifenthaler, D., & Seel, N. M. (2013). Model-based reasoning. *Computers & Education*, 64, 131-142.
- Imamizu, H., & Kawato, M. (2009). Brain mechanisms for predictive control by switching internal models: implications for higher-order cognitive functions. *Psychological Research PRPF*, 73(4), 527-544.
- Ito, M. (2008). Control of mental activities by internal models in the cerebellum. *Nature Reviews Neuroscience*, 9(4), 304-313.
- Janacsek, K., Fiser, J., & Nemeth, D. (2012). The best time to acquire new skills: age-related differences in implicit sequence learning across the human lifespan. *Developmental Science*, 15(4), 496-505.
- Johnson-Laird, P. N., & Byrne, R. M. (1991). *Deduction*. Lawrence Erlbaum Associates, Inc.
- Jueptner, M., Frith, C. D., Brooks, D. J., Frackowiak, R. S. J., & Passingham, R. E. (1997). Anatomy of motor learning. ii. subcortical structures and learning by trial and error. *Journal of Neurophysiology*, 77(3), 1325-37.

- Kable, J. W., & Glimcher, P. W. (2009). The neurobiology of decision: consensus and controversy. *Neuron*, 63(6), 733-745.
- Kahneman, D., & Tversky, A. (1979). Prospect theory: An analysis of decision under risk. *Econometrica*, 47(2), 363-391.
- Kóbor, A., Takács, Á., Janacsek, K., Németh, D., Honbolygó, F., & Csépe, V. (2015). Different strategies underlying uncertain decision making: Higher executive performance is associated with enhanced feedback-related negativity. *Psychophysiology*, 52(3), 367-377.
- Kool, W., Cushman, F. A., & Gershman, S. J. (2016). When does model-based control pay off? *PLoS Computational Biology*, 12(8), e1005090.
- Kool, W., Gershman, S. J., & Cushman, F. A. (2017). Cost-benefit arbitration between multiple reinforcement-learning systems. *Psychological Science*, 28(9), 1321-1333.
- Kuhnen, C. M., & Knutson, B. (2005). The neural basis of financial risk taking. *Neuron*, 47(5), 763-770.
- Laricchiuta, D., Petrosini, L., Piras, F., Macci, E., & Spalletta, G. (2013). Linking novelty seeking and harm avoidance personality traits to cerebellar volumes. *Human Brain Mapping*, 35(1).
- Lee, D., Seo, H., & Jung, M. W. (2012). Neural basis of reinforcement learning and decision making. *Annual Review of Neuroscience*, 35, 287-308.

- Lee, S., Shimojo, S., & J O'Doherty. (2014). Neural computations underlying arbitration between model-based and model-free learning. *Neuron*, 81(3), 687-699.
- Lejuez, C. W., Read, J. P., Kahler, C. W., Richards, J. B., Ramsey, S. E., Stuart, G. L., Brown, R. A. (2002). Evaluation of a behavioral measure of risk taking: The Balloon Analogue Risk Task (BART). *Journal of Experimental Psychology: Applied*, 8(2), 75-84.
- Lemire-Rodger, S., Lam, J., Viviano, J. D., Stevens, W. D., Spreng, R. N., & Turner, G. R. (2019). Inhibit, switch, and update: A within-subject fMRI investigation of executive control. *Neuropsychologia*, 132, 107134.
- Lesage, E., Apps, M. A. J., Hayter, A. L., Beckmann, C. F., Barnes, D., Langdon, D. W., & Ramnani, N. (2010). Cerebellar Information Processing in Relapsing-Remitting Multiple Sclerosis (RRMS). *Behavioural Neurology*, 23(1–2), 39–49.
- Lesage, E., Hansen, P. C., & Miall, R. C. (2017). Right Lateral Cerebellum Represents Linguistic Predictability. *Journal of Neuroscience*, 37(26), 6231–6241.
- Lesage, E., & Verguts, T. (2021). Contextual overtraining accelerates habit formation in new stimuli. In PsyRXiv.
- Li, S., Wen, Q., Yong, L., Wei, H., Zhang, Y., & Jiang, T., et al. (2012). Resting-state functional connectivity of the vermal and hemispheric subregions of the

cerebellum with both the cerebral cortical networks and subcortical structures. *NeuroImage*, 61(4), 1213-1225.

Marek, S., Tervo-Clemmens, B., Calabro, F. J., Montez, D. F., Kay, B. P., Hatoum, A. S., ... & Dosenbach, N. U. (2022). Reproducible brain-wide association studies require thousands of individuals. *Nature*, 603(7902), 654-660.

McCormick, E. M., & Telzer, E. H. (2017). Adaptive adolescent flexibility: neurodevelopment of decision-making and learning in a risky context. *Journal of Cognitive Neuroscience*, 29(3), 413-423.

Miquel, M., Vazquez-Sanroman, D., Carbo-Gas, M., Gil-Miravet, I., & Coria-Avila, G. A. (2016). Have we been ignoring the elephant in the room? seven arguments for considering the cerebellum as part of addiction circuitry. *Neuroscience & Biobehavioral Reviews*, 60(1), 1-11.

Ogilvie, J. M., Shum, D. H., & Stewart, A. (2020). Executive functions in late adolescence and early adulthood and their relationship with risk-taking behavior. *Developmental Neuropsychology*, 45(7-8), 446-468.

O'Reilly, J. X., Beckmann, C. F., Tomassini, V., Ramnani, N., & Johansen-Berg, H. (2010). Distinct and overlapping functional zones in the cerebellum defined by resting state functional connectivity. *Cerebral Cortex*, 20(4), 953–965.

Otto, A.R., Gershman, S.J., Markman, A.B., Daw, N.D. (2013a). The curse of planning dissecting multiple reinforcement-Learning systems by taxing the central executive. *Psychological Science*, 24, 751–761.

- Otto, A.R., Raio, C.M., Chiang, A., Phelps, E.A., Daw, N.D. (2013b). Working-memory capacity protects model-based learning from stress. *Proceedings of the National Academy of Sciences, U. S. A.*, 110, 20941–20946.
- Otto, A. R., Skatova, A., Madlon-Kay, S., & Daw, N. D. (2015). Cognitive Control Predicts Use of Model-based Reinforcement Learning. *Journal of Cognitive Neuroscience*, 27, 319–333.
- Panno, A., Pierro, A., & Lauriola, M. (2014). Self-regulation predicts risk-taking through people's time horizon. *International Journal of Psychology*, 49(3), 211-215.
- Peters, E. M., Bowen, R., & Balbuena, L. (2020). Mood instability and trait anxiety as distinct components of eysenckian neuroticism with differential relations to impulsivity and risk taking. *Journal of Personality Assessment*, 102(3), 337-347.
- Petrosini, L., Cutuli, D., Picerni, E., & Laricchiuta, D. (2015). Cerebellum and personality traits. *The Cerebellum*, 14(1), 43-46.
- Pierro, A., Leder, S., Mannetti, L., Tory Higgins, E., Kruglanski, A. W., & Aiello, A. (2008). Regulatory mode effects on counterfactual thinking and regret. *Journal of Experimental Social Psychology*, 44(2), 321-329.
- Potter, T. C., Bryce, N. V., & Hartley, C. A. (2017). Cognitive components underpinning the development of model-based learning. *Developmental Cognitive Neuroscience*, 25, 272-280.

Power, J. D., Barnes, K. A., Snyder, A. Z., Schlaggar, B. L., & Petersen, S. E. (2012).

Spurious but systematic correlations in functional connectivity MRI networks

arise from subject motion. *NeuroImage*, 59(3), 2142–2154.

Power, J. D., Barnes, K. A., Snyder, A. Z., Schlaggar, B. L., & Petersen, S. E. (2013).

Steps toward optimizing motion artifact removal in functional connectivity MRI;

a reply to carp. *NeuroImage*, 76, 439–441.

Preacher, K. J., & Hayes, A. F. (2008). Asymptotic and resampling strategies for

assessing and comparing indirect effects in multiple mediator models. *Behavior*

Research Methods, 40(3), 879-891.

Quan, P., He, L., Mao, T., Fang, Z., Deng, Y., Pan, Y., ... & Rao, H. (2022).

Cerebellum anatomy predicts individual risk-taking behavior and risk

tolerance. *NeuroImage*, 254, 119148.

van Ravenzwaaij, D., Dutilh, G., & Wagenmakers, E. J. (2011). Cognitive model

decomposition of the BART: Assessment and application. *Journal of*

Mathematical Psychology, 55(1), 94-105.

Rao, H., Korczykowski, M., Pluta, J., Hoang, A., & Detre, J. A. (2008). Neural

correlates of voluntary and involuntary risk taking in the human brain: an fMRI

Study of the Balloon Analog Risk Task (BART). *NeuroImage*, 42(2), 902-910.

Rescorla, R. A., & Wagner, A. (1972). A theory of Pavlovian conditioning: Variations

in the effectiveness of reinforcement and nonreinforcement. *Classical*

Conditioning II: Current Research and Theory, 64-99.

- Rigoux, L., Stephan, K. E., Friston, K. J., & Daunizeau, J. (2014). Bayesian model selection for group studies—revisited. *NeuroImage*, 84, 971-985.
- Ridgway, G. R., Omar, R., Ourselin, S., Hill, D. L., Warren, J. D., & Fox, N. C. (2009). Issues with threshold masking in voxel-based morphometry of atrophied brains. *NeuroImage* 44, 99-111.
- Romer, D., Reyna, V. F., & Satterthwaite, T. D. (2017). Beyond stereotypes of adolescent risk taking: Placing the adolescent brain in developmental context. *Developmental Cognitive Neuroscience*, 27, 19-34.
- Romer, D., Betancourt, L. M., Brodsky, N. L., Giannetta, J. M., Yang, W., & Hurt, H. (2011). Does adolescent risk taking imply weak executive function? A prospective study of relations between working memory performance, impulsivity, and risk taking in early adolescence. *Developmental Science*, 14(5), 1119–1133.
- Saad, Z. S., Gotts, S. J., Murphy, K., Chen, G., Jo, H. J., Martin, A., & Cox, R. W. (2012). Trouble at rest: how correlation patterns and group differences become distorted after global signal regression. *Brain Connectivity*, 2(1), 25-32.
- Schacter, D. L., Addis, D. R., Hassabis, D., Martin, V. C., Spreng, R. N., & Szpunar, K. K. (2012). The future of memory: remembering, imagining, and the brain. *Neuron*, 76(4), 677-694.
- Schonberg, T., Fox, C. R., Mumford, J. A., Congdon, E., Trepel, C., & Poldrack, R. A. (2012). Decreasing ventromedial prefrontal cortex activity during sequential

- risk-taking: an fMRI investigation of the balloon analog risk task. *Frontiers in Neuroscience*, 6, 80.
- Seger, C. A. (2018). Corticostriatal foundations of habits. *Current Opinion in Behavioral Sciences*, 20, 153-160.
- Smittenaar, P., FitzGerald, T. H., Romei, V., Wright, N. D., & Dolan, R. J. (2013). Disruption of dorsolateral prefrontal cortex decreases model-based in favor of model-free control in humans. *Neuron*, 80(4), 914-919.
- Song, Q. C., Tang, C., & Wee, S. (2021). Making sense of model generalizability: A tutorial on cross-validation in R and Shiny. *Advances in Methods and Practices in Psychological Science*, 4(1), 2515245920947067.
- Song, X. W., Dong, Z. Y., Long, X. Y., Li, S. F., Zuo, X. N., Zhu, C. Z., Zang, Y. F. (2011). REST: a toolkit for resting-state functional magnetic resonance imaging data processing. *PLoS One*, 6(9), e25031.
- Stephan, K. E., Penny, W. D., Daunizeau, J., Moran, R. J., & Friston, K. J. (2009). Bayesian model selection for group studies. *NeuroImage*, 46(4), 1004-1017.
- Stoianov, I. P., Pennartz, C. M., Lansink, C. S., & Pezzulo, G. (2018). Model-based spatial navigation in the hippocampus-ventral striatum circuit: A computational analysis. *PLoS Computational Biology*, 14(9), e1006316.
- Stoodley, C. J., Valera, E. M., & Schmahmann, J. D. (2010). An fMRI study of intra-individual functional topography in the human cerebellum. *Behavioural Neurology*, 23(1, 2), 65-79.

- Studer, B., Pedroni, A., & Rieskamp, J. (2013). Predicting Risk-Taking Behavior from Prefrontal Resting-State Activity and Personality. *PLoS One*, 8, e76861.
- Tian, G., Li, B., & Cheng, Y. (2022). Does digital transformation matter for corporate risk-taking? *Finance Research Letters*, 49, 103107.
- Verdejo-García, A., Lawrence, A. J., & Clark, L. (2008). Impulsivity as a vulnerability marker for substance-use disorders: review of findings from high-risk research, problem gamblers and genetic association studies. *Neuroscience & Biobehavioral Reviews*, 32(4), 777-810.
- Watabe-Uchida, M., Eshel, N., & Uchida, N. (2017). Neural Circuitry of Reward Prediction Error. *Annual Review of Neuroscience*, 40, 373–394.
- Weinstein, M. S. (1969). Achievement motivation and risk preference. *Journal of Personality and Social Psychology*, 13(2), 153.
- Yan, C., & Zang, Y. (2010). DPARSF: a MATLAB toolbox for " pipeline" data analysis of resting-state fMRI. *Frontiers in Systems Neuroscience*, 4, 1377.
- Zhou, F., Geng, Y., Xin, F., Li, J., Feng, P., Liu, C., ... & Becker, B. (2019). Human extinction learning is accelerated by an angiotensin antagonist via ventromedial prefrontal cortex and its connections with basolateral amygdala. *Biological Psychiatry*, 86(12), 910-920.
- Zwosta, K., Ruge, H., Goschke, T., & Wolfensteller, U. (2018). Habit strength is predicted by activity dynamics in goal-directed brain systems during training. *NeuroImage*, 165, 125-137.

Figure Captions

Figure 1 Structure of the two-step task with deterministic transitions. The participants need to find treasure by choosing one of the two animals that would bring them to a treasure chest. The animals are linked in pairs: animals enclosed by solid circles would always receive the same value reward from the treasure chest; likewise for animals enclosed by dashed circles.

Figure 2 Behavioral results (191 participants). Bottom left panel: Scatterplot of model-based weighting parameter (ω) and the risk-taking scores (mean adjusted pumps) on the BART. The weighting parameter ω was significantly positively correlated with risk-taking ($r = 0.170, p < 0.05$). Top panel: Histogram of risk-taking scores. Right panel: Histogram of the weighting parameter ω .

Figure 3 VBM results for model-based learning. The GM volumes in (a) the right cerebellum (RCere; MNI center coordinates: 15, -39, -36; Cluster size = 170 voxels; SVC-based $p_{\text{FWE-corr}}=0.025$, SVC corrected), and (b) left inferior parietal lobule (LIPL; MNI center coordinates: -36, -25.5, 34.5; Cluster size = 232 voxels; SVC-based $p_{\text{FWE-corr}}=0.015$, SVC corrected) were positively correlated with the model-based weighting parameter ω .

Figure 4 Resting-state functional connectivity results between the right cerebellum (RCere) seed region of interest identified in the present VBM analysis and other brain areas that correlated with the weighting parameter ω . Functional connectivity between

seed ROIs and left caudate (LCAU) (a) and left inferior parietal lobule (LIPL) (b) were both positively correlated with the weighting parameter ω (voxel significance: $p < 0.005$, cluster significance: $p < 0.05$, GRF corrected).

Figure 5 Mediation results. The effect of the weighting parameter ω on risk-taking (measured by BART) was completely mediated by the association between right cerebellum (RCere) connectivity with the left caudate (LCAU). *: $p < 0.05$; ** $p < 0.01$; ***: $p < 0.001$